

Automated freezing of gait assessment with marker-based motion capture and deep learning approaches expert-level detection

Benjamin Filtjens, Pieter Ginis, Alice Nieuwboer, Peter Slaets, and Bart Vanrumste

Abstract—Freezing of gait (FOG) is a common and debilitating gait impairment in Parkinson’s disease. Further insight in this phenomenon is hampered by the difficulty to objectively assess FOG. To meet this clinical need, this paper proposes a motion capture-based FOG assessment method driven by a novel deep neural network. The proposed network, termed multi-stage graph convolutional network (MS-GCN), combines the spatial temporal graph convolutional network (ST-GCN) and the multi-stage temporal convolutional network (MS-TCN). The ST-GCN captures the hierarchical motion among the optical markers inherent to motion capture, while the multi-stage component reduces over-segmentation errors by refining the predictions over multiple stages. The proposed model was validated on a dataset of fourteen freezers, fourteen non-freezers, and fourteen healthy control subjects. The experiments indicate that the proposed model outperforms state-of-the-art baselines. An in-depth quantitative and qualitative analysis demonstrates that the proposed model is able to achieve clinician-like FOG assessment. The proposed MS-GCN can provide an automated and objective alternative to labor-intensive clinician-based FOG assessment.

I. INTRODUCTION

COMPARED to other neurological disorders, Parkinson’s disease (PD) has a fast growing prevalence, doubling every 20-30 years [1]. Freezing of gait (FOG) is a common and debilitating gait impairment of PD. Up to 80% of the people with Parkinson’s disease (PwPD) will develop FOG during the course of the disease [2], [3]. FOG leads to sudden blocks in walking and is clinically defined as a “brief, episodic absence or marked reduction of forward progression of the feet despite the intention to walk and reach a destination” [4]. The PwPD themselves describe freezing of gait as “the feeling that their feet are glued to the ground” [5]. Freezing episodes most frequently occur while traversing under environmental constraints, during emotional stress, during cognitive overload by means of dual-tasking, and when initiating gait [6], [7]. Though, turning hesitation was found to be the most frequent trigger of FOG [8], [9]. Subjects with FOG experience more anxiety [10], have a lower quality of life [11], and are at a much higher risk of falls [12], [13], [14], [15], [16]. Given the severe adverse effects associated with FOG, there is

a large incentive to advance novel interventions for FOG [17]. The gold standard pharmaceutical intervention for FOG is Levodopa. While Levodopa has shown an overall positive effect on FOG [8], the relationship between FOG and Levodopa remains complex as several studies have indicated that Levodopa often only elicits a partial response and may even exacerbate FOG [18], [19]. Non-pharmaceutical interventions, such as sensory cueing, have also shown an overall positive effect on FOG [20], [21], [22], [23], [24]. Sensory cueing aims to regulate the disturbed stride placement and stride timing inherent to FOG by means of spatial, auditory, or somatosensory stimuli [25].

Unfortunately, the pathophysiology of FOG is complex and the development of novel treatments is severely limited by the difficulty to objectively assess FOG [26]. Due to heightened levels of attention, it is difficult to elicit FOG in the gait laboratory or clinical setting [7], [5]. Therefore, health professionals relied on subjects’ answers to subjective self-assessment questionnaires [27], [28], which may be insufficiently reliable to detect FOG severity [29]. Visual analysis of regular RGB videos or of the 3D images from a motion capture (MoCap) system, have been put forward as the gold standard for rating FOG severity [30], [29], [31]. However, the visual analysis relies on labor-intensive manual annotation by a trained clinical expert. As a result, there is a clear need for an automated and objective approach to assess FOG.

The percentage time spent frozen (%TF), defined as the cumulative duration of all FOG episodes divided by the total duration of the walking task, and number of FOG episodes (#FOG) have been put forward as reliable outcome measures to objectively assess FOG [32]. An accurate segmentation in-time of the FOG episodes, with minimal over-segmentation errors, are required to robustly determine both outcome measures. Prior work have tackled automated FOG assessment by classifying fixed duration input windows [33], [34], [35], [36], [37], [38], [39], [40], [41], [42], [43], [44], [45]. The input windows were then classified with methods ranging from simple thresholding methods [33], [36] to high-level temporal models driven by deep learning [37], [40], [42], [43]. The duration of the window size is a trade-off between expressivity, i.e. the ability to capture long term temporal patterns, and sensitivity, i.e. the ability to identify short-duration FOG episodes. As a result, several papers have aimed to determine the optimal duration of the sliding-window [33], [46], [47], with values typically ranging from half a second to five seconds. The duration of FOG, however, can vary

B. Filtjens and B. Vanrumste are with the eMedia Research Lab/STADIUS, Department of Electrical Engineering (ESAT), KU Leuven, Leuven, 3000, Belgium. e-mail: benjamin.filtjens@kuleuven.be.

B. Filtjens and P. Slaets are with the Intelligent Mobile Platform Research Group, Department of Mechanical Engineering, KU Leuven, 3000, Belgium.

P. Ginis and A. Nieuwboer are with the Research Group for Neurorehabilitation (eNRGy), Department of Rehabilitation Sciences, KU Leuven, Heverlee, 3001, Belgium.

substantially [8]. Furthermore, FOG tends to be preceded by degraded movement [48] and is terminated at the sample prior to two consecutive gait cycles [30]. The sliding-window FOG assessment approaches are only able to exploit local context and do not exploit the long-term temporal patterns that may precede and succeed FOG.

This is the first work to tackle FOG segmentation in MoCap trials of variable duration, a task termed "action segmentation" in the computer vision literature. Several methods have been proposed to tackle action segmentation. Similar to FOG assessment, earlier studies made use of sliding-window classifiers [49], [50], which do not capture long-term temporal patterns [51]. Other approaches use temporal models such as hidden Markov models (HMM) [52], [53] and recurrent neural networks [54], [55]. The state-of-the-art methods tend to use temporal convolutional neural networks (TCN), which have shown to outperform recurrent methods [51], [56]. Dilation is frequently added to capture long-term temporal patterns by expanding the temporal receptive field of the TCN models [57].

In multi-stage temporal convolutional network (MS-TCN), the authors show that multiple stages of temporal dilated convolutions significantly reduce over-segmentation errors [58]. These action segmentation methods have historically been validated on video-based datasets [59], [60] and thus employ video-based features [61].

However, MoCap describes the 3D movement of optical markers in-time, where each marker represents the 3D coordinates of the corresponding anatomical landmark. The human skeleton structure that is inherent to MoCap is not exploited by prior work in action segmentation. To model the structured information among the markers, this paper uses the spatial-temporal graph convolutional neural network (ST-GCN) [62] as the first stage of a MS-TCN network. ST-GCN applies spatial graph convolutions on the human skeleton graph at each time step, and applies dilated temporal convolutions on the temporal edges that connect the same markers across consecutive time steps. The proposed model, termed multi stage graph convolutional neural network (MS-GCN), thus extends MS-TCN to skeleton-based data for automated FOG assessment.

The MS-GCN was tasked to classify segments of FOG in a MoCap dataset. The predicted segments were quantitatively and qualitatively assessed versus the agreed upon annotations by two clinical-expert raters. From the predicted segments, two clinically relevant FOG outcomes, the %TF and #FOG, were computed and statistically validated. Moreover, the importance of the MS-GCN components, i.e. the initial stage of ST-GCN layers and multiple stages of TCN refinements, was assessed through ablation studies.

The proposed MS-GCN is a novel neural network architecture for skeleton-based action segmentation in general and FOG segmentation in particular. The benefit of MS-GCN for FOG assessment is five-fold: (1) It exploits ST-GCN to model the structured information inherent to skeleton data in general and motion-capture data in particular. (2) It allows modelling of long-term temporal context to capture the complex dynamics that precede and succeed FOG. (3) It can operate on high

TABLE I
SUBJECT CHARACTERISTICS.

	Controls	Non-freezers	Freezers	Freezers
Age	65 \pm 6.8	67 \pm 7.4	69 \pm 7.4	67 \pm 9.3
PD duration		7.8 \pm 4.8	9.0 \pm 4.8	10 \pm 6.3
MMSE [63]	29 \pm 1.3	29 \pm 1.2	28 \pm 1.1	28 \pm 1.3
UPDRS III [64]		34 \pm 9.9	38 \pm 14	39 \pm 12
H&Y [65]		2.4 \pm 0.3	2.5 \pm 0.5	2.4 \pm 0.5

temporal resolutions for fine-grained FOG segmentation with precise temporal boundaries. (4) To accomplish (2) and (3) with minimal over-segmentation errors, MS-GCN utilizes multiple stages of refinements, which in turn obviates the need for an a-priori segmentation in fixed duration sliding windows. (5) The proposed segmentations by MS-GCN allow for direct calculation of two clinically relevant FOG outcome measures, namely the %TF and #FOG.

II. METHODS

A. Dataset

Two existing MoCap datasets [30], [66] were included for analysis. The first dataset [30], includes forty-two subjects. Twenty-eight of the subjects were diagnosed with PD by a movement disorders neurologist. Fourteen of the PwPD were classified as freezers based on the first question of the New Freezing of Gait Questionnaire (NFOG-Q): "Did you experience "freezing episodes" over the past month?" [28]. The remaining fourteen subjects were age-matched healthy controls. The second dataset [66], includes seventeen PwPD and FOG, as classified by the NFOG-Q. The subjects underwent a gait assessment at baseline and after twelve months follow-up. Five subjects only underwent baseline assessment and four subjects dropped out during the follow-up. The clinical characteristics are presented in Table I. In the table, left of the vertical line denotes the subject characteristics of the fourteen healthy control subjects (controls), fourteen PwPD and without FOG (non-freezers), and fourteen PwPD and FOG (freezers) of dataset 1. Right of the vertical line denotes the subject characteristics of the seventeen PwPD and FOG (freezers) of dataset 2 at the baseline assessment. All characteristics are given in terms of mean \pm SD. For dataset 1, the characteristics were measured during the ON-phase of the medication cycle, while for dataset 2 the characteristics were measured while OFF medication.

B. Protocol

Both datasets were recorded with a Vicon 3D motion analysis system recording at a sample frequency of 100 Hz. Retro-reflective markers were placed on anatomical landmarks according to the full-body or lower-limb plug-in-gait model [67], [68]. Both datasets featured a nearly identical standardized gait assessment protocol, where two retro-reflective markers placed .5 m from each other indicated where subjects either had to walk straight ahead, turn 360° left, or turn 360° right. For dataset 1, the subjects were additionally instructed to turn

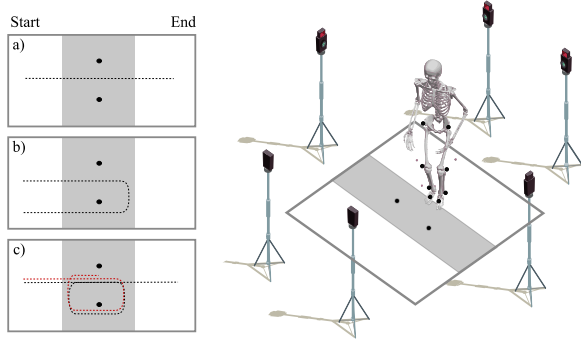


Fig. 1. Overview of the acquisition protocol. Two reflective markers were placed in the middle of the walkway at .5m distance from each other to demarcate the turning radius. The data collection included straight-line walking (a), 180 degree turning (b), and 360 degree turning (c). The protocol was standardized by demarcating a zone of 1m before and 1m after the turn in which data was collected. The gray shaded area visualizes the data collection zone, while the dashed lines indicate the trajectory walked by the subjects. For dataset 2, the data collection only included straight-line walking and 360 degree turning. Furthermore, the data collection ended as soon as the subject completed the turn, as visualized by the red dashed line.

180° left and turn 180° right. The experimental conditions were offered randomly and performed with or without a verbal cognitive dual-task [69], [70]. All gait assessments were conducted during the off-state of the subjects' medication cycle, i.e. after an overnight withdrawal of their normal medication intake. The experimental conditions are visualized in Fig 3.

For dataset 1, two clinical experts, blinded for NFOG-Q score, annotated all FOG episodes by visual inspection of the knee-angle data (flexion-extension) in combination with the MoCap 3D images. For dataset 2, the FOG episodes were annotated by one of the authors (BF) based on visual inspection of the MoCap 3D images. To ensure that the results were unbiased, dataset 2 was used to enrich the training dataset and not for evaluation of the model. For both datasets, the onset of FOG was determined at the heel strike event prior to delayed knee flexion. The termination of FOG was determined at the foot-off event that is succeeded by at least two consecutive movement cycles [30].

C. Temporal FOG segmentation

MoCap describes the 3D movement of optical markers in-time, where each marker represents the 3D coordinates of the corresponding anatomical landmark. The duration of a MoCap trial can vary substantially due to high inter- and intra-subject variability. The goal is to segment a FOG episode in time, given a variable length MoCap trial. The MoCap trial can be represented as $X \in \mathbb{R}^{N \times T \times d}$, where N specifies the number of optical markers, T the number of samples, and d the feature dimension. Each MoCap trial X is associated with a ground truth label vector Y_{exp}^T . The label vector was one-hot encoded and represents the manual annotation of FOG and functional gait by the clinical experts. A deep neural network segments a FOG episode in time by learning a function $f : X \rightarrow Y$ that transforms a given input sequence $X = x_0, \dots, x_T$ into an output sequence $\hat{Y} = \hat{y}_0, \dots, \hat{y}_T$ that closely resembles the manual annotations Y_{exp} .

The marker coordinates were low-pass filtered with a cut-off frequency of 7 Hz using a forward-backward fourth-order butter-worth filter. From the 3D marker coordinates, the marker displacement between two consecutive samples was computed as: $X(n, t+1, :) - X(n, t, :)$. The two markers on the femur and tibia, which were wand markers in dataset 1 and thus placed away from the primary axis, were excluded. The heel marker was excluded due to close proximity with the ankle marker. The reduced marker configuration consists of nine optical markers. The temporal resolution, which was recorded at a sample frequency of 100 HZ, was downsampled to 50 Hz. For action segmentation, reducing the temporal resolution was found to reduce over-segmentation errors at the cost of losing some precision in determining the temporal boundaries [58]. As a result, an input sequence $X \in \mathbb{R}^{N \times T \times d}$ is composed of nine optical markers (N), variable duration (T), and with the feature dimension (d) composed of the 3D displacement of each marker.

To tackle the problem of FOG segmentation, this paper proposes a novel neural network architecture. The proposed neural network, combines the spatial temporal graph convolutional neural network (ST-GCN) [62] with multi-stage refinements introduced in MS-TCN [58]. The proposed architecture was termed multi-stage graph convolutional network (MS-GCN) and is visualized in figure 2. This section introduces each component of the architecture and concludes with implementation details.

1) *ST-GCN*: The ST-GCN introduced in 2018 by Yan et al. [62] generalizes the GCN framework [71] to skeleton-based data. The ST-GCN uses a spatiotemporal graph $G = (V, E)$ to model the structured information among the markers along both the spatial and temporal dimensions. In the spatiotemporal graph, the node set is defined as:

$$V = \{v_{ti} | t = 1, \dots, T, i = 1, \dots, N\}, \quad (1)$$

for a MoCap sequence with N markers and T samples. The feature vector on a node $F(v_{ti})$ of the i -th marker and t -th frame consist of the 3D displacement vectors.

In the spatiotemporal graph, the edge set is composed of two subsets. (1) The spatial dimension, which refers to the intra-skeleton edges at each frame, defined as:

$$E_S = \{v_{ti}v_{tj} | (i, j) \in H\}, \quad (2)$$

where H is the set of connected markers. (2) The temporal dimension, which refers to the inter-frame connection of the same markers over all of the frames, defined as:

$$E_F = \{v_{ti}v_{(t+1)i}\}. \quad (3)$$

Figure 2 presents an example of the constructed spatiotemporal graph. The black markers represent the node set V , the natural connection between markers in a single frame represents the intra-skeleton edges E_S (Fig. 2a), and the marker trajectory over time represents the inter-frame edges E_F (Fig. 2b).

Given the spatiotemporal graph, the graph convolution for a single frame is performed as:

$$f_{out} = \sum_k \Lambda_k^{-\frac{1}{2}} A_k \Lambda_k^{-\frac{1}{2}} f_{in} W_k, \quad (4)$$

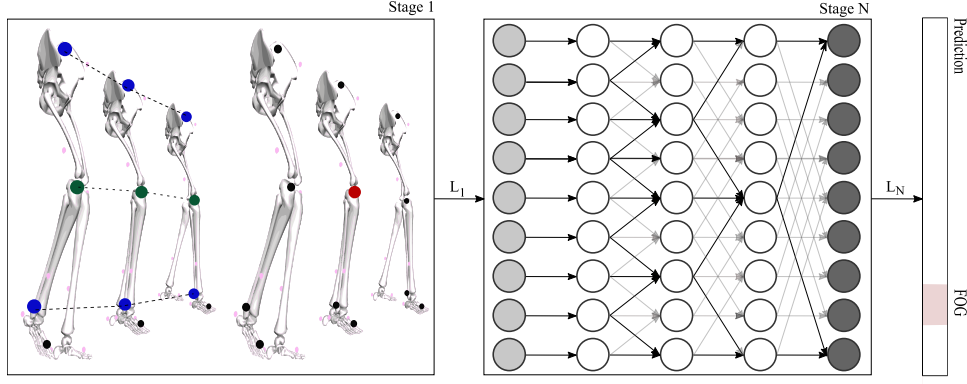


Fig. 2. Overview of the multi stage graph convolutional neural network architecture (MS-GCN). Similar with the traditional MS-TCN, the MS-GCN consists of several stages of dilated 1D convolutions, where each stage generates an initial prediction (dark gray nodes). These predictions are refined in subsequent stages by applying dilated 1D convolutions (white nodes) to the activations of the previous stage (light gray nodes). Different from the traditional MS-TCN, the MS-GCN generates an initial prediction by replacing the dilated 1D convolutions in the first stage with multiple layers of ST-GCN. The ST-GCN layers exploit the skeleton hierarchical structure by limiting the application of each convolution in the spatial domain to the root marker (green) and the nearest neighbour marker (blue), and in the temporal domain to the inter-frame edges (dashed lines).

where f_{out} is the output feature map, $f_{in} \in \mathbb{R}^{T \times N \times C}$ the input feature map with C input channels, and W_k the weight matrix. The connection between nodes is defined in an adjacency matrix $A_k \in \{0, 1\}^{N \times N}$ and normalized adjacency matrix $\Lambda_k^{ii} = \sum_k (A_k^{ij}) + \alpha$. The term α was set to 0.001 to avoid empty rows in Λ_k . The term K denotes the number of different subsets based on the distance-based partitioning function [62]. The distance-based partitioning function consists out of two subsets. The first subset consists of the root nodes with distance 0, while the second subset consists of their neighboring nodes with distance 1, as illustrated in Fig. 2c. Given that $K = 2$, there are two different weight vectors W_k that allow modelling of relative properties between markers [62].

Since the temporal graph is constructed by connecting consecutive frames, ST-GCN uses regular 1D convolutions on the temporal dimensions. A residual connection [72] is added to the ST-GCN layers and dilation [57] is added to the temporal dimension of the ST-GCN layers to alleviate the degradation problem and to expand the temporal receptive field, respectively. With a stride of one for each convolution and adequate padding, the temporal dimension is kept intact throughout the convolutions. As a result, the output feature maps have the same size as the input feature maps. This extension generalizes the ST-GCN, which was originally developed for activity recognition, to activity segmentation on variable length MoCap sequences.

2) *MS-GCN*: In 2019 Farha and Gall [58] show that by stacking multiple stages of temporal 1D convolutions the activity segmentation performance improves. The idea is that each stage refines the predictions from the previous stage. Each stage of the MS-TCN consists of several layers of temporal 1D convolutions. To each layer, the authors also add a residual connection and dilation. The layers were termed as "dilated residual layer". The last layer of each stage is followed by a 1x1 convolution and a softmax activation. As a result,

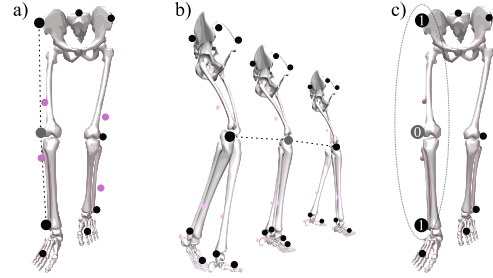


Fig. 3. Left (a): Illustration of the spatial graph. The black markers denote the nodes of the graph and the pink markers denote the unused lower-body plug-in gait markers. The dashed lines illustrate the intra-frame edges (bones) of the root node. Middle (b): Illustration of the temporal graph. The dashed line illustrates the inter-frame edges of the root node between three consecutive timesteps. Right (c): Illustration of the distance partitioning strategy. The first subset is the root node with distance 0 (knee marker), while the second subset is the neighboring points with distance 1 (ankle and hip markers).

later stages operate directly on the softmax activations of the previous stage. Unlike the MS-TCN, the MS-GCN proposed in this paper replaces the dilated residual layers in the initial stage with multiple layers of ST-GCN. Given that the later stages operate on the per-frame softmax activations, i.e. grid-like input data, the incremental refinements in the later stages by means of regular temporal 1D convolutions remain unchanged. To train the neural network, this paper used the same loss as MS-TCN which utilized a combination of a classification loss (cross-entropy) and smoothing loss (mean squared error) for each stage. The combined loss is defined as:

$$L = L_{cls} + \lambda L_{T-MSE}, \quad (5)$$

where the hyperparameter λ controls the contribution of each loss function. The classification loss L_{cls} is the cross entropy loss:

$$L_{cls} = \frac{1}{T} \sum_t -y_{exp,t,c} * \log(y_{t,c}). \quad (6)$$

The smoothing loss L_{T-MSE} is a truncated mean squared error of the frame-wise log-probabilities:

$$L_{T-MSE} = \frac{1}{TC} \sum_{t,c} \tilde{\Delta}_{t,c}^2 \quad (7)$$

$$\tilde{\Delta}_t = \begin{cases} \Delta_{t,c} & : \Delta_{t,c} \leq \tau, \\ \tau & : \text{otherwise}, \end{cases}$$

$$\Delta_{t,c} = |\log y_{t,c} - \log y_{t-1,c}|.$$

In each loss function, T are the number of samples and $y_{t,c}$ is the probability of FOG or functional gait ($C=2$) at sample t . To train the entire network, the sum of the losses over all stages is minimized:

$$L = \sum_s L_s \quad (8)$$

3) *Implementation details:* In the first stage, each layer, i.e., ST-GCN layers in the (proposed) MS-GCN model and dilated residual layers in the MS-TCN model, had 128 convolutional filters with a temporal kernel size of 5. In the refinement stages, each temporal residual layer had 64 convolutional filters with a kernel size of 3. Each stage had 8 layers that applied dilated convolutions with ReLU activation to the output of the previous layer. The input markers were fed into a batch normalization layer to normalize the data. The convolutions were acausal, i.e. they could take into account both past and future input features, with a dilation factor that doubled at each layer, i.e. 1, 2, 4, ..., 128, as illustrated in Fig. 2. To mitigate overfitting, dropout [73] is applied in each layer with a probability of 0.2. For the loss function, τ was set to 4 and λ was set to 0.15. All experiments used the Adam optimizer [74] with a learning rate of 0.0005. To allow an unbiased comparison, the model and optimizer hyperparameters were selected according to MS-TCN [58]. All models thus shared the same hyperparameters and were trained end-to-end with back-propagation for 100 epochs.

D. Evaluation

For dataset 1, FOG was provoked for ten of the fourteen freezers during the test period, with seven subjects freezing within visibility of the MoCap system. For dataset 2, eight of the seventeen freezers froze in visibility of the MoCap system. The training dataset consists of the FOG and non-FOG trials of the seven subjects who froze in-front of the MoCap system of dataset 1, enriched with the FOG trials of the eight subjects who froze in-front of the MoCap system of dataset 2. Only the FOG trials of dataset 2 were considered to balance out the number of FOG and FG trials. Only the subjects of dataset 1 were considered for evaluation, as motivated in the procedure. The evaluation dataset was partitioned according to a leave-one-subject-out cross validation approach. This cross validation approach repeatedly splits the data according to the number of subjects in the dataset. One subject is selected for evaluation, while the other subjects are used to train the model. This procedure is repeated until all subjects have been used for evaluation. This approach mirrors the clinically relevant scenario of FOG assessment in newly recruited subjects [75],

where the model is tasked to assess FOG in unseen subjects. From a machine learning perspective, action segmentation papers tend to use sample-wise metrics, such as the accuracy, precision, and recall. However, sample-wise metrics do not heavily penalize over-segmentation errors. As a result, methods with significant qualitative differences, as was observed between the single stage ST-GCN and MS-GCN, can still achieve similar accuracy. In 2016 Lea et al. [51] proposed a segmental F1-score to address those drawbacks. The segmental F1-score penalizes over-segmentation errors while allowing for minor temporal shifts that may have been caused by annotator variability. In addition, the segmental F1-score is not impacted by the variability in FOG duration, since it is dependent on the number of FOG episodes and not their duration. This paper reports both the frame-wise accuracy and the F1-score at overlapping thresholds of 10, 25, 50, 75, and 90. Both metrics are reported since the discrepancy between frame-wise accuracy and F1-score at overlapping thresholds allows assessment of potential over-segmentation errors. Conclusions were based on the F1-score at high overlap, which correlates the most with the FOG outcomes. For the model validation, the entirety of dataset 1 was used, i.e. MoCap trials without FOG and MoCap trials with FOG, of the seven subjects who froze during the protocol. The machine learning metrics were used to evaluate MS-GCN with respect to the state-of-the-art baselines. While a high number of trials without FOG can inflate the metrics, correct classification of FOG and non FOG segments are, however, of equal importance for assessing FOG severity and thus also for assessing the performance of a machine learning model. To further assess potential false-positive scoring, an additional analysis was performed on trials without FOG of the healthy controls, non-freezers, and freezers that did not freeze during the protocol.

From a clinical perspective, FOG severity is typically assessed in terms of percentage time frozen (%TF) and number of detected FOG episodes (#FOG) [32]. The %TF quantifies the duration of FOG relative to the trial duration, and is defined as:

$$\%TF = \left(\frac{1}{T} \sum_t y_{FOG} \right) * 100, \quad (9)$$

where T are the number of samples in a MoCap trial and y_{FOG} are the FOG samples predicted by the model or the samples annotated by the clinical experts. To evaluate the goodness of fit, the linear relationship between observations by the clinical experts and the model predictions was assessed. Two-sided paired t-tests were computed to evaluate the null hypothesis that the experts annotations and model predictions are not linearly related. The strength of the linear relationship was classified according to [76]: ≥ 0.8 : strong, $0.6 - 0.8$: moderately strong, $0.3 - 0.5$: fair, and < 0.3 : poor. The correlation describes the linear relationship between the experts observations and the model predictions but ignores bias in predictions. Therefore, a two-sided paired t-test was computed to evaluate the null hypothesis that the mean difference between the experts annotations and model predictions (experts-model) is zero. The significance level for all tests was set at 0.05. For the statistical analysis, only the trials with

FOG were considered, as trials without FOG would inflate the reliability scores.

III. RESULTS

A. MS-GCN: ablation studies

The first experiment aimed to dissect the effectiveness of the proposed components, i.e., the initial stage of multiple ST-GCN layers and the multi stage refinements, through ablation studies. The performance was assessed for 1-6 refinement stages, where a stage of 1 corresponds to a single-stage model. All these models were run on variable length motion capture trials, with the 3D displacement of nine optical markers as input features. All models were trained using a leave-one-subject-out cross-validation approach and used the same hyper parameters. The metrics were summarized in terms of mean \pm standard deviation (SD) of the seven subjects that froze during the protocol, where the SD aims to capture the variability across different subjects.

According to the results shown in table II, the ST-GCN based models outperform the TCN based models on all evaluation metrics. This result confirms the notion that graph convolutions give a better representation of skeleton-based data than regular temporal convolutions [62]. Additionally, the multi-stage refinements improve the f1 score at several overlapping thresholds, the metric that penalize over-segmentation errors. This result confirms the notion that multi-stage refinements can improve the performance of neural network models for fine-grained activity segmentation [58]. Though, for FOG segmentation the improvement starts to flatten out after more than 2 refinement stages.

The second experiment aims to dissect the importance of the dilated and acausal convolutions. The results are quantified in table III, where the asterisk (*) denotes the MS-GCN without dilated convolutions and the dagger (†) denotes the MS-GCN without acausal convolutions. According to the results shown in table III, dilated and acausal convolutions are crucial architectural elaborations for accurate FOG segmentation. These findings may indicate the importance of long-term past and future temporal context for determining precise temporal FOG boundaries.

B. Qualitative comparison with the baseline models

For the two subjects (S5 and S7) that froze only during one MoCap trial, the proposed segmentation of the MS-GCN and baseline models are visualized in figure 5. For these trials, video renders in OpenSim [77] are provided in appendix. The renders allow the reader to visually verify the observations made in this analysis. According to figure 5, the single stage ST-GCN model detects all freezing episodes. However, the proposed segmentations demonstrate over-segmentation errors, which would inflate the clinical outcome #FOG. This finding explains the aforementioned quantitative results of table II, where the single stage ST-GCN performed similarly on the sample-wise accuracy but worse on the two segmentation metrics. On the other hand, the MS-TCN model ameliorates the over-segmentation problems. However, the proposed segmentations fail to capture two of the FOG episodes. The

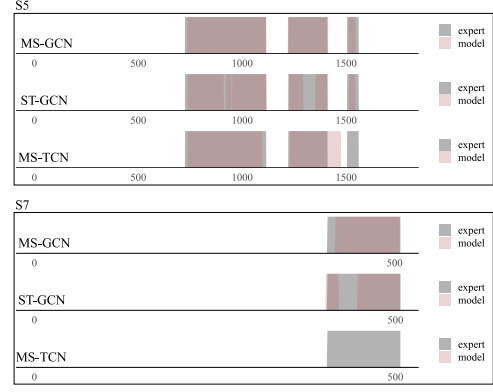


Fig. 4. Overview of two standardized motion capture trials, visualizing the difference between the manual FOG segmentation by the clinician and automated FOG segmentation by (1) MS-GCN (6 stages), (2) ST-GCN (1 stage), and (3) MS-TCN (6 stages). For each of the two subjects, the first trial is the proposed segmentation by MS-GCN, the second by ST-GCN, and the last by MS-TCN. The x-axis denotes the number of samples (at a sample frequency of 100hz). The color gradient visualizes the overlap or discrepancy between the model and experts annotations. The two presented trials were extracted from the two freezers that froze once during the protocol. Video renders for these trials are included in the appendix. All model annotations were derived from the test set, i.e., subjects that the models have never seen.

proposed MS-GCN seems to effectively combine the positives of each method and results in a near-perfect FOG assessment for these two subjects. These qualitative findings support the previous quantitative results and confirm that the multi-stage model reduces over-segmentation errors, while the graph convolutions are a crucial extension to model the structured spatial temporal information among the optical markers.

C. Automated FOG assessment: statistical analysis and subject specific results

The clinical experts observed at least one FOG episode in 35 MoCap trials of dataset 1. The number of detected FOG episodes (#FOG) per trial varied from 1 to 5 amounting to 56 FOG episodes, while the percentage time frozen (%TF) varied from 4.2 to 75. For the %TF, the model predictions had a very strong linear relationship with the experts observations, with a correlation value [95 % CI] of $r=0.95$ [0.91, 0.98] ($t=18$, $p=2.2e^{-16}$). For the #FOG, the model predictions had a moderately strong linear relationship with the experts' observations, with a correlation value [95 % CI] of $r=0.74$ [0.53, 0.86] ($t=6.3$, $p=4.6e^{-7}$). For both outcomes, the null hypothesis should be rejected ($p < 0.05$), i.e., the linear relationship between the model predictions and the experts' annotations is statistically significant. The linear relationship is visualized in figure 5. Two-sided paired t-tests were computed to check if the predictions had proportional bias. The bias [95 % CI] was found to be -1.6 [-3.8, 0.59] ($t=-1.5$, $p=0.15$) and -0.51 [-1.1, 0.07] ($t=-1.8$, $p=0.08$) for %TF and #FOG, respectively. MS-GCN overestimated the %TF and #FOG. Though, the p value was higher than 0.05, indicating that there was no statistical evidence to reject the null hypothesis that states that the mean difference between the model predictions and the experts annotations is zero.

Automated FOG assessment performance varied highly between subjects. The subject-specific results are quantified in

TABLE II
ABLATION STUDY: EFFECT OF THE NUMBER OF STAGES AND GRAPH CONVOLUTIONS.

Model	acc \pm SD	f1@10 \pm SD	f1@25 \pm SD	f1@50 \pm SD
ST-GCN (1 stage)	97.1 \pm 3.09	80.3 \pm 17.0	79.9 \pm 17.6	76.3 \pm 20.0
TCN (1 stage)	87.4 \pm 16.0	77.5 \pm 21.3	74.6 \pm 23.8	69.7 \pm 27.1
MS-GCN (2 stages)	97.6 \pm 2.40	88.2 \pm 10.6	87.8 \pm 11.2	85.8 \pm 12.8
MS-TCN (2 stages)	88.6 \pm 15.3	82.4 \pm 17.2	79.5 \pm 21.0	72.1 \pm 26.9
MS-GCN (3 stages)	97.6 \pm 2.29	88.8 \pm 7.45	88.0 \pm 7.26	85.6 \pm 9.30
MS-TCN (3 stages)	89.9 \pm 13.0	82.4 \pm 15.2	79.6 \pm 19.6	73.7 \pm 22.7
MS-GCN (4 stages)	97.7 \pm 2.37	90.3 \pm 8.70	89.5 \pm 9.57	86.7 \pm 11.0
MS-TCN (4 stages)	89.4 \pm 14.1	83.2 \pm 16.5	79.8 \pm 19.7	73.3 \pm 25.3
MS-GCN (5 stages)	97.6 \pm 2.30	88.8 \pm 8.32	87.6 \pm 8.34	85.8 \pm 9.92
MS-TCN (5 stages)	88.9 \pm 14.7	85.0 \pm 12.8	81.1 \pm 17.7	76.5 \pm 22.2
MS-GCN (6 stages)	97.5 \pm 2.42	89.9 \pm 7.56	89.7 \pm 7.88	87.3 \pm 9.69
MS-TCN (6 stages)	88.8 \pm 15.0	83.8 \pm 14.8	80.9 \pm 19.2	76.0 \pm 23.1

TABLE III
ABLATION STUDY: EFFECT OF THE DILATED AND ACAUSAL CONVOLUTIONS.

Model	acc \pm SD	f1@10 \pm SD	f1@25 \pm SD	f1@50 \pm SD
MS-GCN*	97.2 \pm 2.88	84.3 \pm 19.0	83.8 \pm 19.6	80.6 \pm 21.9
MS-GCN†	97.2 \pm 2.79	82.4 \pm 15.2	81.7 \pm 16.5	79.0 \pm 18.6
MS-GCN	97.5 \pm 2.42	89.9 \pm 7.56	89.7 \pm 7.88	87.3 \pm 9.69

The asterisk (*) denotes the MS-GCN without dilated convolutions.

The dagger (†) denotes the MS-GCN without acausal convolutions.

terms of the sample-wise accuracy (acc) and f1 scores at overlapping thresholds of 10, 25, 50, 75, and 90 (f1@10, f1@25, f1@50, f1@75, f1@90). The letter k denotes the number of extracted standardized motion capture trials and the letter l denotes the number of those motion capture trials with FOG. According to table IV, the F1 score at 50% overlap (f1@50) varied from 76% to 100%, while the mean \pm SD was found to be $87\% \pm 9.7\%$.

A quantitative assessment of the MS-GCN predictions for the fourteen healthy control subjects (controls), fourteen non-freezers (non-freezers), seven freezers who did not freeze during the protocol (freezers-), and the non-freezing trials of the seven freezers who did freeze during the protocol (freezers+) demonstrates the robustness of the automated FOG assessment. The results are summarized in table V, where the letter n denotes the number of subjects and the letter k denotes the number of extracted standardized motion capture trials. According to table V, no false positive FOG segments were predicted.

D. Qualitative analysis of model and experts discrepancies

The statistical and quantitative FOG severity results indicated a discrepancy between automated FOG assessment by the MS-GCN and the manual FOG assessment by the two clinical experts. A qualitative analysis was performed which aims to dissect an explanation for the discrepancy. The proposed FOG segmentation by the model and experts are visualized in Fig 6 for all trials with FOG in the dataset. Five MoCap trials, one of each of the five subjects not

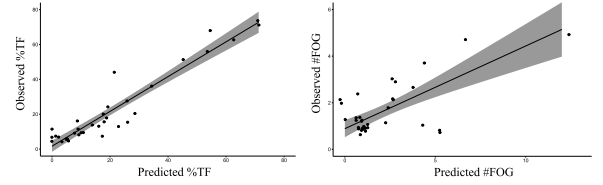


Fig. 5. Assessing the performance of the MS-GCN (6 stages) for automated FOG assessment. More specifically, the performance to measure the percentage time frozen (%TF) (left) and the number of FOG episodes (#FOG) (right) during a standardized protocol. All results were derived from the test set, i.e., subjects that the model had never seen.

discussed in the previous section, are visualized in Fig 6 and qualitatively analysed. These five trials best capture the discrepancy between automated FOG segmentation by the MS-GCN and manual FOG segmentation by the clinical experts. For these trials, video renders in OpenSim [77] are provided in the appendix. The renders allow the reader to visually verify the observations made in this analysis. Moreover, for each discussed trial, the relative percentage difference between the model and experts %TF is given.

Fig 6, S1 shows the FOG segmentation for one of the MoCap trials of subject S1. For the chosen MoCap trial, the model performed the worst with a relative percentage difference of 14%. According to the figure, the model and experts demarcated the start of the FOG episode around the same sample. A slight discrepancy between model and experts can be observed in demarcating the end of the FOG episode, with the model slightly extending the FOG episode. According to the video, the subject demonstrated complete akinesia during

TABLE IV
SUBJECT-SPECIFIC RESULTS.

Subject ID	acc	f1@10	f1@25	f1@50	f1@75	f1@90
S1 (k=28, l=3)	98.5	90.9	90.9	88.6	88.6	84.1
S2 (k=22, l=11)	95.2	81.3	79.7	78.1	67.2	54.7
S3 (k=27, l=4)	99.2	88.2	88.2	85.3	85.3	76.5
S4 (k=21, l=10)	93.9	85.7	85.7	75.7	61.4	51.4
S5 (k=24, l=1)	99.7	100	100	100	96.7	96.7
S6 (k=7, l=5)	95.9	83.3	83.3	83.3	66.7	50.0
S7 (k=31, l=1)	99.9	100	100	100	100	95.4
Mean \pm SD	97.5 \pm 2.42	89.9 \pm 7.56	89.7 \pm 7.88	87.3 \pm 9.69	80.8 \pm 15.6	72.7 \pm 20.5

TABLE V
MS-GCN ROBUSTNESS.

Subjects	FP
Controls (n=14, k=404)	0
Non-freezers (n=14, k=423)	0
Freezers- (n=7, k=195)	0
Freezers+ (n=7, k=125)	0

the episode, succeeded by trembling in place before resuming functional gait. The experts demarcated the end of the FOG episode prior to the trembling in place, while the model included two of the trembling strides as part of the FOG episode.

Fig 6, S2 shows the FOG segmentation for one of the MoCap trials of subject S2. For the chosen MoCap trial, the model performed the worst with a relative percentage difference of 134%. According to the figure, the model severely overestimates the number of FOG episodes, with the model and experts only agreeing on the FOG episode between sample 2500 and 3000 at the end of the 360 degree turn. According to the video, the subject demonstrated small shuffling steps during turning, with the FOG episode at the end of the 360 degree turn characterised by trembling in place. Furthermore, the subject shows three moments of interrupted forward progression. Two moments around the 180 degree of the turn and one prior to the agreed upon FOG episode near the end of the turn. The model annotated these moments as FOG, while the experts did not.

Fig 6, S3 shows the FOG segmentation for one of the MoCap trials of subject S3. The chosen MoCap trial, with a relative percentage difference of 67%, best indicates the discrepancy between model and experts for this subject. According to the figure, the model severely underestimates the duration of the FOG episode. Therefore, this prediction would be considered a false negative at thresholds ≥ 0.5 . According to the video, the subject demonstrated small shuffling steps during turning, with a sudden sub-second FOG episode that is characterised by trembling in place. Furthermore, the subject demonstrates a stooped gait signature without apparent reduction of movement in the stride directly preceding FOG and strides that occurred further away from the FOG episode. In all of the MoCap trials with FOG, the model either fails to detect the episodes or underestimates their duration. An experiment was carried

out where MS-GCN was exposed to the subjects' unique gait signature by means of transfer learning with a small learning rate (learning rate = 0.0001, epochs = 50, batch size = 1). The results of this experiment are visualized in Figure 7. It can be observed that after transfer learning, the proposed segmentation by MS-GCN greatly improved.

Fig 6, S4 shows the FOG segmentation for one of the MoCap trials of subject S4. The selected trial had a relative percentage difference of 12%. According to the figure, a near perfect segmentation is observed for FOG episode 2-4. However, the model underestimates the duration of the first FOG episode. According to the video, the FOG episode(s) leading up to the turn occur suddenly without prior reduction of movement and are characterised by complete akinesia. During the turn, the subject demonstrated small shuffling steps, with trembling in place occurring during the FOG episode(s). The model picks up the first episode after the subject has taken two strides of degraded movement, while the experts detects the episode immediately.

Fig 6, S6 shows the FOG segmentation for one of the MoCap trials of subject S6. The chosen trial had a relative percentage difference of 46%. According to the video, the subject demonstrated small shuffling steps during turning, with the FOG episode characterised by trembling in place. According to the figure, the model did not pick up the short FOG episode at 180 degrees in the turn. In addition, the model underestimates the duration of the second FOG episode by detecting the FOG episode two impaired strides later than the experts.

IV. DISCUSSION

This paper presented MS-GCN, a novel neural network architecture for automated and objective FOG assessment in variable length MoCap trials. MS-GCN extends MS-TCN [58], the state-of-the-art model in action segmentation, to graph-based input data that is inherent to MoCap. To model the hierarchical spatiotemporal motion of the optical MoCap markers, MS-GCN replaces the first stage of regular 1D temporal convolutions with several layers of ST-GCN [62], the state-of-the-art model in skeleton-based action detection. Unlike prior work in automated FOG assessment, where the temporal receptive field is limited to the duration of pre-defined sliding-windows, the temporal receptive field of MS-GCN is defined by the model architecture itself. To capture long-term temporal patterns, MS-GCN utilizes dilated convolutions [57]. The dilated convolutions expand the temporal receptive

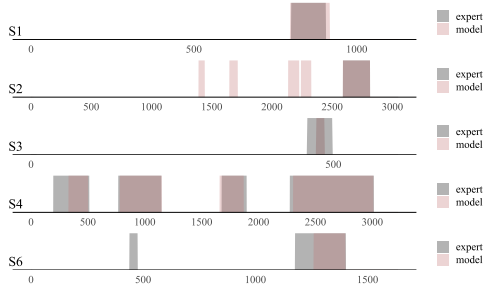


Fig. 6. Overview of five standardized motion capture trials, visualizing the difference between the manual FOG segmentation by the clinician and the automated FOG segmentation by the MS-GCN (6 stages). The x-axis denotes the number of samples (at a sample frequency of 100Hz). The color gradient visualizes the overlap or discrepancy between the model and experts annotations. For each of the five presented trials, from five unique freezers, a video render is included in the appendix. The model annotations were derived from the test set, i.e., subjects that the model had never seen.

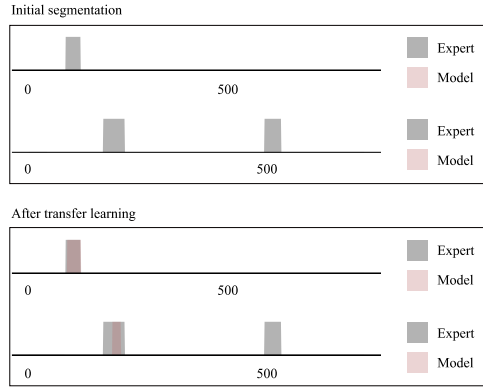


Fig. 7. Overview of the transfer learning results for the two motion capture trials of S3. For these two trials, MS-GCN initially failed to detect FOG due to subjects' unique gait and FOG signature. It can be observed that the proposed segmentation greatly improves after exposing MS-GCN to the subjects' unique gait and FOG signature. The initial segmentation is visualized in the top figure, while the segmentation after transfer learning is visualized in the bottom figure.

field, which allows MS-GCN to model FOG according to the threshold model, which states that freezing is characterized by a continuous degradation of the movement pattern until a threshold is reached and the FOG episode occurs [48]. To take into account future observations, MS-GCN utilizes acausal convolutions. The acausal convolutions aim to capture the termination of FOG, defined as the sample that precedes two functional cycles [30], which requires future (acausal) observations to determine accurately.

In-depth ablation studies were performed to assess the contribution of the proposed extensions. The ablation studies quantified the model performance using typical machine learning metrics used in the action segmentation literature [58], [51]. For the two main contributions, i.e. the combination of multi stage refinements and graph convolutions, a qualitative analysis was performed which aimed to serve as a visual confirmation for the quantitative results of the ablation studies. The analyses confirmed the aforementioned notions that: (1) the multi-stage refinements reduce over-segmentation errors, and (2) that the graph convolutions give a better representation

of skeleton-based data than regular temporal convolutions. In addition, dilated and acausal convolutions were found to be crucial architectural elaborations for accurate FOG segmentation.

Two common outcome measures to assess FOG, the %TF and #FOG [32], were computed and statistically assessed. MS-GCN showed a very strong ($r=0.95$) and moderately strong ($r=0.74$) linear relationship with the experts observations for %TF and #FOG, respectively. Furthermore, no statistically significant bias was observed for either metric. For context, the intraclass correlation coefficient between independent assessors was reported to be 0.87 [78] and 0.73 [32] for %TF and 0.63 [32] for #FOG.

A qualitative analysis was performed which aimed to dissect the discrepancy between MS-GCN and the clinical experts. The analysis indicated that the primary cause of discrepancy is that the MS-GCN typically proposes a more fine-grained segmentation than the experts. This cause is in line with the main discrepancy between clinical experts described in earlier work [32]. Given that the training dataset consists out of: (1) the agreed upon labels of two clinical experts for dataset 1, and (2) the labels by one of the authors for dataset 2, it is not unsurprising that MS-GCN models this discrepancy. Furthermore, the proposed fine-grained segmentation of MS-GCN often highlights very brief FOG segments which are not picked-up by the experts. Annotation of these segments are typically also the tedious parts of FOG assessment which consume most of the rating time. It is likely that if the expert raters are pointed at these brief FOG segments, the experts may agree with the MS-GCN segmentation.

A benefit of MS-GCN is that it is not strictly limited to marker-based MoCap data. The MS-GCN architecture naturally extends to other graph-based input data, such as single- or multi-camera markerless pose estimation [79], [80], and FOG assessment protocols that employ multiple on-body sensors [34], [35]. Both technologies are receiving increased attention due to the potential to assess FOG not only in the lab, but also in an at-home environment and thereby better capture daily-life FOG severity. Furthermore, up til now deep learning based gait assessment [81], [82], [83], including our own [84], did not yet exploit the inherent graph structured data. The established breakthrough in FOG assessment by this research might, therefore, signify further breakthroughs in deep learning-based gait assessment in general.

Several limitations are present. The first and most prominent limitation is the lack of variety in the standardized FOG provoking protocol. FOG is characterized by several apparent subtypes, such as turning and destination hesitation, and gait initiation [8]. While turning was found to be the most prominent [8], [9], it should still be established whether MS-GCN can generalize to other FOG subtypes under different FOG provoking protocols. For now, practitioners are advised to closely follow the experimental protocol used in this study when employing MS-GCN. The second limitation is the small sample size. While MS-GCN was evaluated based on the clinically relevant use-case scenario of FOG assessment in newly recruited subjects, the sample size of the dataset is relatively small compared to the deep learning literature. The third

limitation is based on the observation that FOG assessment in the clinic and lab is prone to two shortcomings. (1) FOG can be challenging to elicit in the lab due to elevated levels of attention [5], [7], despite providing adequate FOG provoking circumstances [30], [85]. (2) Research has demonstrated that FOG severity in the lab is not necessarily representative of FOG severity in daily-life [86], [5]. Future work should therefore establish whether the proposed method can generalize to tackle automated FOG assessment with on-body sensors or markerless MoCap captured in less constrained environments. Fourth, MS-GCN seemed to perform worse for S3, with the model failing to detect FOG in half of the MoCap trials where the subject froze. As demonstrated in the video renders, this subject has a very characteristic gait and FOG signature. An experiment was carried out where MS-GCN was exposed to the subjects' unique gait signature by means of transfer learning. The results indicated that after transfer learning, the proposed segmentation by MS-GCN greatly improved. While the sample size is too small to be definitive, this phenomenon may indicate that personalization of MS-GCN can lead to improved FOG assessment for subjects with a unique gait or FOG signature. Fifth, due to opaqueness inherent to deep learning, clinicians have historically distrusted DNNs [87]. However, prior case studies [88], have demonstrated that interpretability techniques are able to visualize what features the model has learned [89], [90], [91], which can aid the clinician in determining whether the assessment was based on credible features. Lastly, a direct comparison with prior work in automated FOG detection is difficult due to different underlying study designs. Instead, an in-depth quantitative and qualitative comparison was performed with state of the art baselines in action segmentation.

V. CONCLUSION

FOG is a debilitating motor impairment of PD. Unfortunately, our understanding of this phenomenon is hampered by the difficulty to objectively assess FOG. To tackle this problem, this paper proposed a novel deep neural network architecture. The proposed architecture, termed MS-GCN, was quantitatively and qualitatively validated versus the expert clinical opinion of two independent raters. In conclusion, it can be established that MS-GCN demonstrates expert-like FOG assessment performance. Furthermore, future work is now possible that aims to assess the generalization of MS-GCN to other graph-based input data, such as markerless MoCap or multiple on-body sensor configurations, and to other FOG subtypes captured under less constrained protocols. Such work is important to increase our understanding of this debilitating phenomenon during everyday life.

ADDITIONAL INFORMATION

A. Data availability

The input set was imported and labelled using Python version 2.7.12 with Biomechanical Toolkit (btk) version 0.3 [92]. The MS-GCN architecture was implemented in Pytorch version 1.2 [93] by adopting the public code repositories of MS-TCN [58] and ST-GCN [62]. All models were trained on

an NVIDIA Tesla K80 GPU using Python version 3.6.8. The video renders were created with OpenSim [77]. The datasets analysed during the current study are not publicly available due to restrictions on sharing subject health information.

REFERENCES

- [1] E. R. Dorsey, R. Constantinescu, J. P. Thompson, K. M. Biglan, R. G. Holloway, K. Kiebert, F. J. Marshall, B. M. Ravina, G. Schifitto, A. Siderowf, and C. M. Tanner, "Projected number of people with parkinson disease in the most populous nations, 2005 through 2030," *Neurology*, vol. 68, no. 5, pp. 384–386, Jan. 2007.
- [2] S. Perez-Lloret, L. Negre-Pages, P. Damier, A. Delval, P. Derkinderen, A. Destée, W. G. Meissner, L. Schelosky, F. Tison, and O. Rascol, "Prevalence, determinants, and effect on quality of life of freezing of gait in parkinson disease," *JAMA Neurol.*, vol. 71, no. 7, pp. 884–890, Jul. 2014.
- [3] M. A. Hely, W. G. J. Reid, M. A. Adena, G. M. Halliday, and J. G. L. Morris, "The sydney multicenter study of parkinson's disease: the inevitability of dementia at 20 years," *Mov. Disord.*, vol. 23, no. 6, pp. 837–844, Apr. 2008.
- [4] J. G. Nutt, B. R. Bloem, N. Giladi, M. Hallett, F. B. Horak, and A. Nieuwboer, "Freezing of gait: moving forward on a mysterious clinical phenomenon," *Lancet Neurol.*, vol. 10, no. 8, pp. 734–744, Aug. 2011.
- [5] A. H. Snijders, M. J. Nijkrake, M. Bakker, M. Munneke, C. Wind, and B. R. Bloem, "Clinimetrics of freezing of gait," *Mov. Disord.*, vol. 23 Suppl 2, pp. S468–74, 2008.
- [6] J. Nonnekes, A. H. Snijders, J. G. Nutt, G. Deuschl, N. Giladi, and B. R. Bloem, "Freezing of gait: a practical approach to management," *Lancet Neurol.*, vol. 14, no. 7, pp. 768–778, Jul. 2015.
- [7] Y. Okuma, "Practical approach to freezing of gait in parkinson's disease," *Pract. Neurol.*, vol. 14, no. 4, pp. 222–230, Aug. 2014.
- [8] J. D. Schaafsma, Y. Balash, T. Gurevich, A. L. Bartels, J. M. Hausdorff, and N. Giladi, "Characterization of freezing of gait subtypes and the response of each to levodopa in parkinson's disease," *Eur. J. Neurol.*, vol. 10, no. 4, pp. 391–398, Jul. 2003.
- [9] N. Giladi, J. Balash, and J. M. Hausdorff, "Gait disturbances in parkinson's disease," in *Mapping the Progress of Alzheimer's and Parkinson's Disease*, Y. Mizuno, A. Fisher, and I. Hanin, Eds. Boston, MA: Springer US, 2002, pp. 329–335.
- [10] N. Giladi and J. M. Hausdorff, "The role of mental function in the pathogenesis of freezing of gait in parkinson's disease," *J. Neurol. Sci.*, vol. 248, no. 1–2, pp. 173–176, Oct. 2006.
- [11] O. Moore, S. Kreidler, M. Ehrenfeld, and N. Giladi, "Quality of life and gender identity in parkinson's disease," *J. Neural Transm.*, vol. 112, no. 11, pp. 1511–1522, Nov. 2005.
- [12] B. R. Bloem, J. M. Hausdorff, J. E. Visser, and N. Giladi, "Falls and freezing of gait in parkinson's disease: a review of two interconnected, episodic phenomena," *Mov. Disord.*, vol. 19, no. 8, pp. 871–884, Aug. 2004.
- [13] Y. A. M. Grimbergen, M. Munneke, and B. R. Bloem, "Falls in parkinson's disease," *Curr. Opin. Neurol.*, vol. 17, no. 4, pp. 405–415, Aug. 2004.
- [14] P. Gray and K. Hildebrand, "Fall risk factors in parkinson's disease," *J. Neurosci. Nurs.*, vol. 32, no. 4, pp. 222–228, Aug. 2000.
- [15] M. Rudzińska, S. Bukowczan, J. Stożek, K. Zajdel, E. Mirek, W. Chwata, M. Wójcik-Pedziwiatr, K. Banaszkiewicz, and A. Szczudlik, "Causes and consequences of falls in parkinson disease patients in a prospective study," *Neurol. Neurochir. Pol.*, vol. 47, no. 5, pp. 423–430, Jan. 2013.
- [16] P. H. S. Pelicioni, J. C. Menant, M. D. Latt, and S. R. Lord, "Falls in parkinson's disease subtypes: Risk factors, locations and circumstances," *Int. J. Environ. Res. Public Health*, vol. 16, no. 12, Jun. 2019.
- [17] M. Gilat, A. Lúcia Silva de Lima, B. R. Bloem, J. M. Shine, J. Nonnekes, and S. J. G. Lewis, "Freezing of gait: Promising avenues for future treatment," *Parkinsonism Relat. Disord.*, vol. 52, pp. 7–16, Jul. 2018.
- [18] J. Lucas McKay, F. C. Goldstein, B. Sommerfeld, D. Bernhard, S. Perez Parra, and S. A. Factor, "Freezing of gait can persist after an acute levodopa challenge in parkinson's disease," *NPJ Parkinsons Dis.*, vol. 5, p. 25, Nov. 2019.
- [19] A. J. Espay, A. Fasano, B. F. L. van Nuenen, M. M. Payne, A. H. Snijders, and B. R. Bloem, "on" state freezing of gait in parkinson disease: a paradoxical levodopa-induced complication," *Neurology*, vol. 78, no. 7, pp. 454–457, Feb. 2012.

- [20] I. Lim, E. van Wegen, C. de Goede, M. Deutekom, A. Nieuwboer, A. Willems, D. Jones, L. Rochester, and G. Kwakkel, "Effects of external rhythmic cueing on gait in patients with parkinson's disease: a systematic review," *Clin. Rehabil.*, vol. 19, no. 7, pp. 695–713, Oct. 2005.
- [21] A. Nieuwboer, G. Kwakkel, L. Rochester, D. Jones, E. van Wegen, A. M. Willems, F. Chavret, V. Hetherington, K. Baker, and I. Lim, "Cueing training in the home improves gait-related mobility in parkinson's disease: the RESCUE trial," *J. Neurol. Neurosurg. Psychiatry*, vol. 78, no. 2, pp. 134–140, Feb. 2007.
- [22] T. C. Rubinstein, N. Giladi, and J. M. Hausdorff, "The power of cueing to circumvent dopamine deficits: a review of physical therapy treatment of gait disturbances in parkinson's disease," *Mov. Disord.*, vol. 17, no. 6, pp. 1148–1160, Nov. 2002.
- [23] P. Arias and J. Cudeiro, "Effect of rhythmic auditory stimulation on gait in parkinsonian patients with and without freezing of gait," *PLoS One*, vol. 5, no. 3, p. e9675, Mar. 2010.
- [24] C. Cosentino, M. Baccini, M. Putzolu, D. Ristori, L. Avanzino, and E. Pelosin, "Effectiveness of physiotherapy on freezing of gait in parkinson's disease: A systematic review and Meta-Analyses," *Mov. Disord.*, vol. 35, no. 4, pp. 523–536, Apr. 2020.
- [25] A. Nieuwboer, "Cueing for freezing of gait in patients with parkinson's disease: a rehabilitation perspective," *Mov. Disord.*, vol. 23 Suppl 2, pp. S475–81, 2008.
- [26] M. Mancini, B. R. Bloem, F. B. Horak, S. J. G. Lewis, A. Nieuwboer, and J. Nonnkes, "Clinical and methodological challenges for assessing freezing of gait: Future perspectives," *Mov. Disord.*, vol. 34, no. 6, pp. 783–790, Jun. 2019.
- [27] N. Giladi, H. Shabtai, E. S. Simon, S. Biran, J. Tal, and A. D. Korczyn, "Construction of freezing of gait questionnaire for patients with parkinsonism," *Parkinsonism Relat. Disord.*, vol. 6, no. 3, pp. 165–170, Jul. 2000.
- [28] A. Nieuwboer, L. Rochester, T. Herman, W. Vandenberghe, G. E. Emil, T. Thomaes, and N. Giladi, "Reliability of the new freezing of gait questionnaire: agreement between patients with parkinson's disease and their carers," *Gait Posture*, vol. 30, no. 4, pp. 459–463, Nov. 2009.
- [29] J. M. Shine, S. T. Moore, S. J. Bolitho, T. R. Morris, V. Dilda, S. L. Naismith, and S. J. G. Lewis, "Assessing the utility of freezing of gait questionnaires in parkinson's disease," *Parkinsonism Relat. Disord.*, vol. 18, no. 1, pp. 25–29, Jan. 2012.
- [30] J. Spildooren, S. Vercruysse, K. Desloovere, W. Vandenberghe, E. Kerckhofs, and A. Nieuwboer, "Freezing of gait in parkinson's disease: the impact of dual-tasking and turning," *Mov. Disord.*, vol. 25, no. 15, pp. 2563–2570, Nov. 2010.
- [31] M. Gilat, "How to annotate freezing of gait from video: A standardized method using Open-Source software," *J. Parkinsons. Dis.*, vol. 9, no. 4, pp. 821–824, 2019.
- [32] T. R. Morris, C. Cho, V. Dilda, J. M. Shine, S. L. Naismith, S. J. G. Lewis, and S. T. Moore, "A comparison of clinical and objective measures of freezing of gait in parkinson's disease," *Parkinsonism Relat. Disord.*, vol. 18, no. 5, pp. 572–577, Jun. 2012.
- [33] S. T. Moore, H. G. MacDougall, and W. G. Ondo, "Ambulatory monitoring of freezing of gait in parkinson's disease," *J. Neurosci. Methods*, vol. 167, no. 2, pp. 340–348, Jan. 2008.
- [34] S. T. Moore, D. A. Yungher, T. R. Morris, V. Dilda, H. G. MacDougall, J. M. Shine, S. L. Naismith, and S. J. G. Lewis, "Autonomous identification of freezing of gait in parkinson's disease from lower-body segmental accelerometry," *J. Neuroeng. Rehabil.*, vol. 10, p. 19, Feb. 2013.
- [35] M. B. Popovic, M. Djuric-Jovicic, S. Radovanovic, I. Petrovic, and V. Kostic, "A simple method to assess freezing of gait in parkinson's disease patients," *Braz. J. Med. Biol. Res.*, vol. 43, no. 9, pp. 883–889, Sep. 2010.
- [36] A. Delval, A. H. Snijders, V. Weerdesteyn, J. E. Duysens, L. Defebvre, N. Giladi, and B. R. Bloem, "Objective detection of subtle freezing of gait episodes in parkinson's disease," *Mov. Disord.*, vol. 25, no. 11, pp. 1684–1693, Aug. 2010.
- [37] K. Hu, Z. Wang, S. Mei, K. A. Ehgoetz Martens, T. Yao, S. J. G. Lewis, and D. D. Feng, "Vision-Based freezing of gait detection with anatomic directed graph representation," *IEEE J Biomed Health Inform.*, vol. 24, no. 4, pp. 1215–1225, Apr. 2020.
- [38] C. Ahlrichs, A. Samà, M. Lawo, J. Cabestany, D. Rodríguez-Martín, C. Pérez-López, D. Sweeney, L. R. Quinlan, G. Ó. Laighin, T. Counihan, P. Browne, L. Hadas, G. Vainstein, A. Costa, R. Annicchiarico, S. Alcaine, B. Mestre, P. Quispe, Á. Bayés, and A. Rodríguez-Molinero, "Detecting freezing of gait with a tri-axial accelerometer in parkinson's disease patients," *Med. Biol. Eng. Comput.*, vol. 54, no. 1, pp. 223–233, Jan. 2016.
- [39] D. Rodríguez-Martín, A. Samà, C. Pérez-López, A. Català, J. M. Moreno Arostegui, J. Cabestany, Á. Bayés, S. Alcaine, B. Mestre, A. Prats, M. C. Crespo, T. J. Counihan, P. Browne, L. R. Quinlan, G. Ó. Laighin, D. Sweeney, H. Lewy, J. Azuri, G. Vainstein, R. Annicchiarico, A. Costa, and A. Rodríguez-Molinero, "Home detection of freezing of gait using support vector machines through a single waist-worn triaxial accelerometer," *PLoS One*, vol. 12, no. 2, p. e0171764, Feb. 2017.
- [40] S. Masiala, W. Huijbers, and M. Atzmueller, "Feature-Set-Engineering for detecting freezing of gait in parkinson's disease using deep recurrent neural networks," *pre-print*, Sep. 2019.
- [41] P. Tahafchi, R. Molina, J. A. Roper, K. Sowalsky, C. J. Hass, A. Gunduz, M. S. Okun, and J. W. Judy, "Freezing-of-Gait detection using temporal, spatial, and physiological features with a support-vector-machine classifier," in *2017 39th Annual International Conference of the IEEE Engineering in Medicine and Biology Society (EMBC)*, Jul. 2017, pp. 2867–2870.
- [42] J. Camps, A. Samà, M. Martín, D. Rodríguez-Martín, C. Pérez-López, S. Alcaine, B. Mestre, A. Prats, M. C. Crespo, J. Cabestany, Á. Bayés, and A. Català, "Deep learning for detecting freezing of gait episodes in parkinson's disease based on accelerometers," in *Advances in Computational Intelligence*. Springer International Publishing, 2017, pp. 344–355.
- [43] L. Sigcha, N. Costa, I. Pavón, S. Costa, P. Arezes, J. M. López, and G. De Arcas, "Deep learning approaches for detecting freezing of gait in parkinson's disease patients through On-Body acceleration sensors," *Sensors*, vol. 20, no. 7, Mar. 2020.
- [44] M. Mancini, K. C. Priest, J. G. Nutt, and F. B. Horak, "Quantifying freezing of gait in parkinson's disease during the instrumented timed up and go test," *Conf. Proc. IEEE Eng. Med. Biol. Soc.*, vol. 2012, pp. 1198–1201, 2012.
- [45] M. Mancini, V. V. Shah, S. Stuart, C. Curtze, F. B. Horak, D. Safarpour, and J. G. Nutt, "Measuring freezing of gait during daily-life: an open-source, wearable sensors approach," *J. Neuroeng. Rehabil.*, vol. 18, no. 1, p. 1, Jan. 2021.
- [46] V. Mikos, C. Heng, A. Tay, N. S. Y. Chía, K. M. L. Koh, D. M. L. Tan, and W. L. Au, "Optimal window lengths, features and subsets thereof for freezing of gait classification," in *2017 International Conference on Intelligent Informatics and Biomedical Sciences (ICIBMS)*, Nov. 2017, pp. 1–8.
- [47] A. Samà, D. Rodríguez-Martín, C. Pérez-López, A. Català, S. Alcaine, B. Mestre, A. Prats, M. C. Crespo, and Á. Bayés, "Determining the optimal features in freezing of gait detection through a single waist accelerometer in home environments," *Pattern Recognit. Lett.*, vol. 105, pp. 135–143, Apr. 2018.
- [48] M. Plotnik, N. Giladi, and J. M. Hausdorff, "Is freezing of gait in parkinson's disease a result of multiple gait impairments? implications for treatment," *Parkinsons Dis.*, vol. 2012, p. 459321, Jan. 2012.
- [49] M. Rohrbach, S. Amin, M. Andriluka, and B. Schiele, "A database for fine grained activity detection of cooking activities," in *2012 IEEE Conference on Computer Vision and Pattern Recognition*, Jun. 2012, pp. 1194–1201.
- [50] B. Ni, X. Yang, and S. Gao, "Progressively parsing interactional objects for fine grained action detection," in *2016 IEEE Conference on Computer Vision and Pattern Recognition (CVPR)*, Jun. 2016, pp. 1020–1028.
- [51] C. Lea, M. D. Flynn, R. Vidal, A. Reiter, and G. D. Hager, "Temporal convolutional networks for action segmentation and detection," in *2017 IEEE Conference on Computer Vision and Pattern Recognition (CVPR)*, 2017, pp. 1003–1012.
- [52] H. Kuehne, J. Gall, and T. Serre, "An end-to-end generative framework for video segmentation and recognition," *IEEE Workshop on Applications of Computer Vision (WACV)*, Sep. 2015.
- [53] K. Tang, L. Fei-Fei, and D. Koller, "Learning latent temporal structure for complex event detection," in *2012 IEEE Conference on Computer Vision and Pattern Recognition*, Jun. 2012, pp. 1250–1257.
- [54] B. Singh, T. K. Marks, M. Jones, O. Tuzel, and M. Shao, "A multi-stream bi-directional recurrent neural network for Fine-Grained action detection," in *2016 IEEE Conference on Computer Vision and Pattern Recognition (CVPR)*, Jun. 2016, pp. 1961–1970.
- [55] D.-A. Huang, L. Fei-Fei, and J. C. Niebles, "Connectionist temporal modeling for weakly supervised action labeling," in *Computer Vision – ECCV 2016*, B. Leibe, J. Matas, N. Sebe, and M. Welling, Eds. Cham: Springer International Publishing, 2016, pp. 137–153.
- [56] S. Bai, J. Zico Kolter, and V. Koltun, "An empirical evaluation of generic convolutional and recurrent networks for sequence modeling," *pre-print*, Mar. 2018.

- [57] F. Yu and V. Koltun, "Multi-Scale context aggregation by dilated convolutions," *pre-print*, Nov. 2015.
- [58] Y. A. Farha and J. Gall, "Ms-tcn: Multi-stage temporal convolutional network for action segmentation," in *2019 IEEE/CVF Conference on Computer Vision and Pattern Recognition (CVPR)*, 2019, pp. 3570–3579.
- [59] A. Fathi, X. Ren, and J. M. Rehg, "Learning to recognize objects in egocentric activities," in *CVPR 2011*, Jun. 2011, pp. 3281–3288.
- [60] S. Stein and S. J. McKenna, "Combining embedded accelerometers with computer vision for recognizing food preparation activities," in *Proceedings of the 2013 ACM international joint conference on Pervasive and ubiquitous computing*, ser. UbiComp '13. New York, NY, USA: Association for Computing Machinery, Sep. 2013, pp. 729–738.
- [61] J. Carreira and A. Zisserman, "Quo vadis, action recognition? a new model and the kinetics dataset," in *2017 IEEE Conference on Computer Vision and Pattern Recognition (CVPR)*, 2017, pp. 4724–4733.
- [62] S. Yan, Y. Xiong, and D. Lin, "Spatial temporal graph convolutional networks for skeleton-based action recognition," in *AAAI*, 2018.
- [63] M. F. Folstein, S. E. Folstein, and P. R. McHugh, "“mini-mental state”: a practical method for grading the cognitive state of patients for the clinician," *J. Psychiatr. Res.*, vol. 12, no. 3, pp. 189–198, Nov. 1975.
- [64] C. G. Goetz, B. C. Tilley, S. R. Shaftman, G. T. Stebbins, S. Fahn, P. Martinez-Martin, W. Poewe, C. Sampaio, M. B. Stern, R. Dodel, B. Dubois, R. Holloway, J. Jankovic, J. Kulisevsky, A. E. Lang, A. Lees, S. Leurgans, P. A. LeWitt, D. Nyenhuis, C. W. Olanow, O. Rascol, A. Schrag, J. A. Teresi, J. J. van Hilten, N. LaPelle, and Movement Disorder Society UPDRS Revision Task Force, "Movement disorder society-sponsored revision of the unified parkinson's disease rating scale (MDS-UPDRS): scale presentation and clinimetric testing results," *Mov. Disord.*, vol. 23, no. 15, pp. 2129–2170, Nov. 2008.
- [65] M. M. Hoehn and M. D. Yahr, "Parkinsonism: onset, progression and mortality," *Neurology*, vol. 17, no. 5, pp. 427–442, May 1967.
- [66] G. Vervoor, A. Bengevoord, C. Strouwen, E. M. J. Bekkers, E. Heremans, W. Vandenberghe, and A. Nieuwboer, "Progression of postural control and gait deficits in parkinson's disease and freezing of gait: A longitudinal study," *Parkinsonism Relat. Disord.*, vol. 28, pp. 73–79, Jul. 2016.
- [67] M. P. Kadaba, H. K. Ramakrishnan, and M. E. Wootten, "Measurement of lower extremity kinematics during level walking," *J. Orthop. Res.*, vol. 8, no. 3, pp. 383–392, May 1990.
- [68] R. B. Davis, S. Öunpuu, D. Tyburski, and J. R. Gage, "A gait analysis data collection and reduction technique," *Hum. Mov. Sci.*, vol. 10, no. 5, pp. 575–587, Oct. 1991.
- [69] C. G. Canning, L. Ada, J. J. Johnson, and S. McWhirter, "Walking capacity in mild to moderate parkinson's disease," *Arch. Phys. Med. Rehabil.*, vol. 87, no. 3, pp. 371–375, Mar. 2006.
- [70] A. Bowen, R. Wenman, J. Mickelborough, J. Foster, E. Hill, and R. Tallis, "Dual-task effects of talking while walking on velocity and balance following a stroke," *Age Ageing*, vol. 30, no. 4, pp. 319–323, Jul. 2001.
- [71] T. N. Kipf and M. Welling, "Semi-Supervised classification with graph convolutional networks," *pre-print*, Sep. 2016.
- [72] K. He, X. Zhang, S. Ren, and J. Sun, "Deep residual learning for image recognition," in *2016 IEEE Conference on Computer Vision and Pattern Recognition (CVPR)*, 2016, pp. 770–778.
- [73] N. Srivastava, G. Hinton, A. Krizhevsky, I. Sutskever, and R. Salakhutdinov, "Dropout: A simple way to prevent neural networks from overfitting," *J. Mach. Learn. Res.*, vol. 15, no. 56, pp. 1929–1958, 2014.
- [74] D. P. Kingma and J. Ba, "Adam: A method for stochastic optimization," *pre-print*, Dec. 2014.
- [75] S. Saeb, L. Lonini, A. Jayaraman, D. C. Mohr, and K. P. Kording, "The need to approximate the use-case in clinical machine learning," *Gigascience*, vol. 6, no. 5, pp. 1–9, May 2017.
- [76] Y. H. Chan, "Biostatistics 104: correlational analysis," *Singapore Med. J.*, vol. 44, no. 12, pp. 614–619, Dec. 2003.
- [77] S. L. Delp, F. C. Anderson, A. S. Arnold, P. Loan, A. Habib, C. T. John, E. Guendelman, and D. G. Thelen, "OpenSim: open-source software to create and analyze dynamic simulations of movement," *IEEE Trans. Biomed. Eng.*, vol. 54, no. 11, pp. 1940–1950, Nov. 2007.
- [78] C. C. Walton, L. Mowszowski, M. Gilat, J. M. Hall, C. O'Callaghan, A. J. Muller, M. Georgiades, J. Y. Y. Szeto, K. A. Ehgoetz Martens, J. M. Shine, S. L. Naismith, and S. J. G. Lewis, "Cognitive training for freezing of gait in parkinson's disease: a randomized controlled trial," *NPJ Parkinsons Dis*, vol. 4, p. 15, May 2018.
- [79] Z. Cao, G. Hidalgo, T. Simon, S. E. Wei, and Y. Sheikh, "Openpose: Realtime multi-person 2d pose estimation using part affinity fields," *IEEE Transactions on Pattern Analysis and Machine Intelligence*, vol. 43, no. 1, pp. 172–186, 2021.
- [80] A. Mathis, P. Mamidanna, K. M. Cury, T. Abe, V. N. Murthy, M. W. Mathis, and M. Bethge, "DeepLabCut: markerless pose estimation of user-defined body parts with deep learning," *Nat. Neurosci.*, vol. 21, no. 9, pp. 1281–1289, Aug. 2018.
- [81] Ł. Kidziński, S. Delp, and M. Schwartz, "Automatic real-time gait event detection in children using deep neural networks," *PLoS One*, vol. 14, no. 1, p. e0211466, Jan. 2019.
- [82] Ł. Kidziński, B. Yang, J. L. Hicks, A. Rajagopal, S. L. Delp, and M. H. Schwartz, "Deep neural networks enable quantitative movement analysis using single-camera videos," *Nat. Commun.*, vol. 11, no. 1, p. 4054, Aug. 2020.
- [83] M. Lempereur, F. Rousseau, O. Rémy-Nériss, C. Pons, L. Houx, G. Quellec, and S. Brochard, "A new deep learning-based method for the detection of gait events in children with gait disorders: Proof-of-concept and concurrent validity," *J. Biomech.*, vol. 98, p. 109490, Jan. 2020.
- [84] B. Filtjens, A. Nieuwboer, N. D'cruz, J. Spildooren, P. Slaets, and B. Vanrumste, "A data-driven approach for detecting gait events during turning in people with parkinson's disease and freezing of gait," *Gait Posture*, vol. 80, pp. 130–136, Jul. 2020.
- [85] A. Nieuwboer, R. Dom, W. De Weerd, K. Desloovere, S. Fieuws, and E. Broens-Kaucsik, "Abnormalities of the spatiotemporal characteristics of gait at the onset of freezing in parkinson's disease," *Mov. Disord.*, vol. 16, no. 6, pp. 1066–1075, Nov. 2001.
- [86] S. Rahman, H. J. Griffin, N. P. Quinn, and M. Jahanshahi, "The factors that induce or overcome freezing of gait in parkinson's disease," *Behav. Neurol.*, vol. 19, no. 3, pp. 127–136, 2008.
- [87] A. Barredo Arrieta, N. Díaz-Rodríguez, J. Del Ser, A. Bennetot, S. Tabik, A. Barbado, S. Garcia, S. Gil-Lopez, D. Molina, R. Benjamins, R. Chatila, and F. Herrera, "Explainable artificial intelligence (XAI): Concepts, taxonomies, opportunities and challenges toward responsible AI," *Inf. Fusion*, vol. 58, pp. 82–115, Jun. 2020.
- [88] F. Horst, S. Lapuschkin, W. Samek, K.-R. Müller, and W. I. Schödlhorn, "Explaining the unique nature of individual gait patterns with deep learning," *Sci. Rep.*, vol. 9, no. 1, p. 2391, Feb. 2019.
- [89] S. Bach, A. Binder, G. Montavon, F. Klauschen, K.-R. Müller, and W. Samek, "On Pixel-Wise explanations for Non-Linear classifier decisions by Layer-Wise relevance propagation," *PLoS One*, vol. 10, no. 7, p. e0130140, Jul. 2015.
- [90] M. Sundararajan, A. Taly, and Q. Yan, "Axiomatic attribution for deep networks," in *Proceedings of the 34th International Conference on Machine Learning - Volume 70*, ser. ICML'17. JMLR.org, 2017, p. 3319–3328.
- [91] A. Shrikumar, P. Greenside, and A. Kundaje, "Learning important features through propagating activation differences," in *Proceedings of the 34th International Conference on Machine Learning*, ser. Proceedings of Machine Learning Research, D. Precup and Y. W. Teh, Eds., vol. 70. International Convention Centre, Sydney, Australia: PMLR, 06–11 Aug 2017, pp. 3145–3153. [Online]. Available: <http://proceedings.mlr.press/v70/shrikumar17a.html>
- [92] A. Barre and S. Armand, "Biomechanical ToolKit: Open-source framework to visualize and process biomechanical data," *Comput. Methods Programs Biomed.*, vol. 114, no. 1, pp. 80–87, Apr. 2014.
- [93] A. Paszke, S. Gross, F. Massa, A. Lerer, J. Bradbury, G. Chanan, T. Killeen, Z. Lin, N. Gimelshein, L. Antiga, A. Desmaison, A. Kopf, E. Yang, Z. DeVito, M. Raison, A. Tejani, S. Chilamkurthy, B. Steiner, L. Fang, J. Bai, and S. Chintala, "Pytorch: An imperative style, high-performance deep learning library," in *Advances in Neural Information Processing Systems*, H. Wallach, H. Larochelle, A. Beygelzimer, F. d'Alché-Buc, E. Fox, and R. Garnett, Eds., vol. 32. Curran Associates, Inc., 2019. [Online]. Available: <https://proceedings.neurips.cc/paper/2019/file/bdbca288fee7f92f2bfa9f7012727740-Paper.pdf>